Received: 14 June 2018 | Revised: 12 November 2018 | Accepted: 13 December 2018

DOI: 10.1002/mrm.27654

FULL PAPER

Magnetic Resonance in Medicine

Toward direct MRI of neuro-electro-magnetic oscillations in the human brain

Trong-Kha Truong[1] | **Kenneth C. Roberts**[2] | **Marty G. Woldorff**[2] | **Allen W. Song**[1]

[1]Brain Imaging and Analysis Center, Duke University, Durham, North Carolina

[2]Center for Cognitive Neuroscience, Duke University, Durham, North Carolina

Correspondence
Trong-Kha Truong, 40 Duke Medicine Circle, Room 414, Durham, NC 27710, USA.
Email: trongkha.truong@duke.edu

Funding information
National Institute of Mental Health, Grant/Award Number: R24 MH106048.

Purpose: Neuroimaging techniques are widely used to investigate the function of the human brain, but none are currently able to accurately localize neuronal activity with both high spatial and temporal specificity. Here, a new in vivo MRI acquisition and analysis technique based on the spin-lock mechanism is developed to noninvasively image local magnetic field oscillations resulting from neuroelectric activity in specifiable frequency bands.

Methods: Simulations, phantom experiments, and in vivo experiments using an eyes-open/eyes-closed task in 8 healthy volunteers were performed to demonstrate its sensitivity and specificity for detecting oscillatory neuroelectric activity in the alpha-band (8-12 Hz). A comprehensive postprocessing procedure was designed to enhance the neuroelectric signal, while minimizing any residual hemodynamic and physiological confounds.

Results: The phantom results show that this technique can detect 0.06-nT magnetic field oscillations, while the in vivo results demonstrate that it can image task-based modulations of neuroelectric oscillatory activity in the alpha-band. Multiple control experiments and a comparison with conventional BOLD functional MRI suggest that the activation was likely not due to any residual hemodynamic or physiological confounds.

Conclusion: These initial results provide evidence suggesting that this new technique has the potential to noninvasively and directly image neuroelectric activity in the human brain in vivo. With further development, this approach offers the promise of being able to do so with a combination of spatial and temporal specificity that is beyond what can be achieved with existing neuroimaging methods, which can advance our ability to study the functions and dysfunctions of the human brain.

KEYWORDS
alpha band, functional magnetic resonance imaging, neuroelectric activity, neuronal oscillations, spin-lock

1 | INTRODUCTION

Noninvasive neuroimaging techniques are the most widely used tools to study the structure and function of the human brain in vivo. BOLD functional MRI (fMRI)[1-3] benefits from relatively high spatial resolution and coverage of the whole brain, but it relies on secondary hemodynamic modulations that are only an indirect measure of neuronal activity, and

 © 2019 International Society for Magnetic Resonance in Medicine

with a very low temporal resolution. Conversely, scalp-recorded electroencephalography (EEG)[4] and magnetoencephalography (MEG),[5] which are more direct measures of neural activity, benefit from a high temporal resolution and the ability to capture neuroelectric oscillations. However, they are limited by poor and/or ambiguous spatial resolution, primarily due to the inverse problem for localizing sources of electrical activity in a volume based on measurements on the surface. Multimodal imaging such as simultaneous EEG/fMRI recording can provide complementary information about brain activity, but it cannot truly achieve a high spatial and temporal accuracy simultaneously due to the disparate signal sources. Thus, the development of a neuroimaging technique that can noninvasively and directly image neuroelectric activity with both a high spatial and temporal specificity would greatly advance our ability to study the human brain.

Early attempts at using MRI to detect a phase shift or signal loss caused by electrical currents were successful in phantom[6,7] and in vitro[8-10] experiments. However, in vivo studies in the brain using this approach have remained challenging and controversial,[11-22] because the local magnetic fields induced by neuronal currents are not only extremely weak, but can also be oscillatory, resulting in temporal cancellation within the acquisition window, and because of challenging hemodynamic, respiratory, and cardiac-related confounds. More recently, spin-lock techniques based on the rotary saturation effect,[23] which can be tuned to detect magnetic field oscillations within specific frequency bands, such as those induced by functional neuroelectric currents, have shown promising results in phantoms[24-27] but have not yet been applied successfully in vivo, even in rats.[28]

Here, we report a new spin-lock technique that can reach a level of sensitivity that enables the imaging of neuro-electromagnetic oscillations (NEMO) in the human brain in vivo. We apply this technique and demonstrate its viability and effectiveness, both in phantom experiments and in the human brain in vivo.

2 | METHODS

2.1 | Pulse sequence

The pulse sequence consists of a spin-lock preparation followed by a gradient-echo spiral readout (Figure 1A). Specifically, a 90° RF pulse is first applied along the x'-axis (in the rotating frame rotating about the z-axis at the Larmor frequency), which flips the magnetization **M** from the z'-axis (Figure 1B) to the y'-axis (Figure 1C). To selectively extract oscillatory activity in a specifiable frequency band, a spin-lock pulse also rotating at the Larmor frequency and with a spin-lock frequency ω (with an amplitude $B_{1,\text{spin-lock}}$ such that $\omega = \gamma B_{1,\text{spin-lock}}$) is then applied along the y'-axis. Because the spin-lock field $\mathbf{B}_{1,\text{spin-lock}}$ and the magnetization **M** are both along the y'-axis, **M** is temporarily locked along this axis and rotates around it at the same frequency.[24-27,29]

In the presence of neuroelectric oscillations at the same frequency ω that generate a magnetic field $\mathbf{B}_{z'}$ oscillating

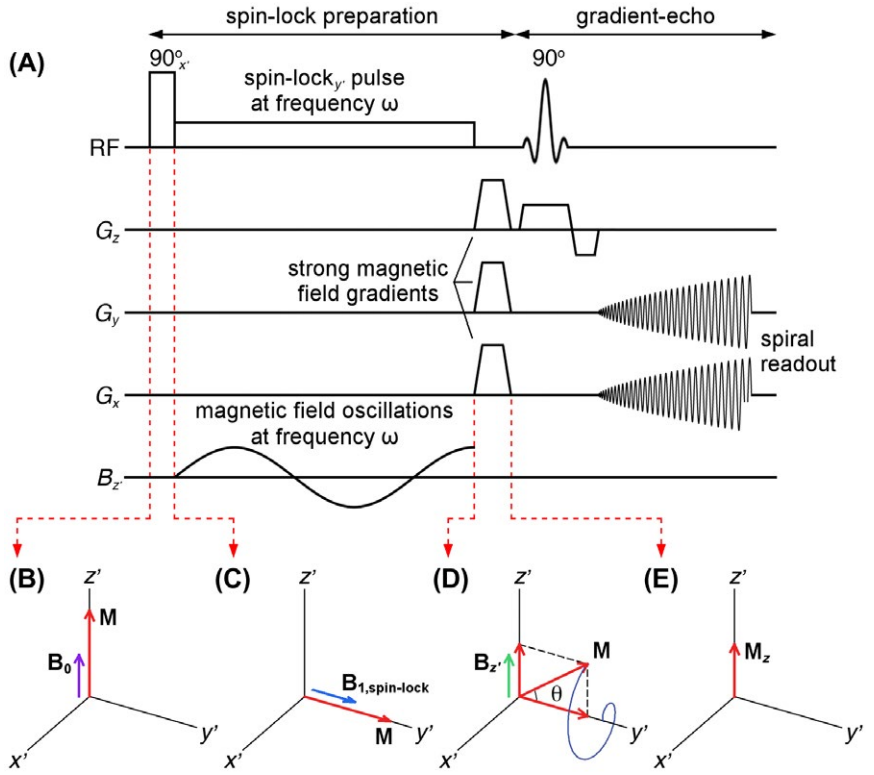

FIGURE 1 A, Pulse sequence diagram consisting of a spin-lock preparation and a gradient-echo spiral readout. Time evolution of the magnetization **M** at the beginning of the pulse sequence (B); after the first 90° pulse, which flips **M** from the z'-axis to the y'-axis (C); after the spin-lock pulse with a spin-lock frequency ω equal to that of the local magnetic field oscillations $\mathbf{B}_{z'}$ induced by neuroelectric activity, which nutate **M** away from the y'-axis by a nutation angle θ (D); and after the strong magnetic field gradients, which eliminate the $M_{x'}$ and $M_{y'}$ components, leaving only the $M_{z'}$ component for subsequent imaging (E). The diagrams in (B-E) are all shown in the rotating frame rotating about the z-axis at the Larmor frequency

between the $+z'$ and $-z'$ axes, **M** gradually nutates away from the y'-axis due to gyromagnetic forces (Figure 1D). The evolution of **M** in the spin-locked state can be described by Equations 1 and 2 from Zhu et al[27] in a doubly rotating frame rotating about the z-axis at the Larmor frequency and about the y'-axis at the spin-lock frequency. This evolution depends on the spin-lattice relaxation time in the spin-locked state, $T_{1\rho}$, which is ~78 ms in the human cortical gray matter at 3T.[30]

Once a sufficient nutation angle θ is reached, the spin-lock pulse is turned off, and strong magnetic field gradients are applied to dephase and eliminate the $M_{x'}$ and $M_{y'}$ components while preserving the $M_{z'}$ component (Figure 1E). The selectively preserved $M_{z'}$ component is then excited by another 90° pulse to generate an MR image with selective sensitivity to the NEMO activity. A spiral-out readout with minimal TE is used, along with a comprehensive postprocessing method (see below), to minimize any residual hemodynamic effects. The NEMO signal is thus distinctly different from the typical MRI signal (including the BOLD signal) that originates from the spin precession at the Larmor frequency pointing only in the $+z'$ direction.

Furthermore, the NEMO signal depends on whether the magnetization **M** at the end of the spin-lock pulse ends up in the y'–z' plane (as shown in Figure 1D), in the x'–y' plane, or somewhere in between, which in turn depends on the phase of the neuroelectric oscillations relative to the spin-lock pulse. This phase dependence can in principle be used to investigate the temporal dynamics of the neuroelectric oscillations in vivo.

The main advantage of our new imaging technique is the boost in SNR resulting from the fact that only the $M_{z'}$ component, which results from the neuroelectric oscillations, is selectively imaged, whereas the $M_{x'}$ and $M_{y'}$ components, as well as other contributions to the magnetization (e.g., due to B_0 inhomogeneities), remain in the transverse plane and are eliminated by the strong magnetic field gradients, thereby effectively suppressing the noise floor. In contrast, previous spin-lock techniques may be confounded by such additional contributions, because they either apply a second 90° pulse after the spin-lock pulse to restore *all* the transverse magnetization to the z'-axis for subsequent excitation[27] or leave it in the transverse plane for subsequent imaging.[26,28] Furthermore, our technique, which uses the sin(θ) component of **M**, benefits from a higher sensitivity for small θ values than the original spin-lock technique,[24,25] which used the (1 – cos(θ)) component, because $\sin(\theta) >> 1 - \cos(\theta)$ for such values.[26,27] For example, if the amplitude of the oscillating magnetic field $B_{z'}$ is 1 nT and the spin-lock duration T_{SL} is 125 ms, the sensitivity is increased by $\sin(\theta)/(1 - \cos(\theta)) \approx 60$, where $\theta = \gamma B_{z'} T_{SL}$.

Like previous spin-lock techniques, our technique is only sensitive to magnetic fields oscillating along the z'-axis, whether the spin-lock pulse is applied along the x'-axis or y'-axis. However, the NEMO signal is expected to be present in most voxels in which there is neuroelectric activity, given that the volume and primary neuronal currents would almost always have a z'-component. Like previous spin-lock techniques, our technique is also theoretically less sensitive to cancellation effects resulting from any spatial heterogeneity of the oscillating magnetic field within a voxel.

2.2 | Phantom MRI experiments

To demonstrate the specificity, sensitivity, and oscillatory-phase dependence of this technique, we performed phantom experiments by applying an oscillating current in a water phantom and varying its frequency, amplitude, and phase relative to the spin-lock pulse. These experiments were performed on a 3T MR750 MRI scanner (GE Healthcare, Milwaukee, WI) with an 8-channel head coil. A 3-cm diameter axial wire loop taped outside a 10-cm diameter spherical water phantom doped with $NiCl_2$ was connected through a twisted-pair cable and a variable resistor to a sine-wave function generator, which was triggered by the scanner to control the phase of the oscillating current relative to the spin-lock pulse.

Images were acquired with our spin-lock technique in an axial slice 1 cm away from the loop, with TE = 3 ms, FOV = 12 × 12 cm, matrix size = 64 × 64, in-plane spatial resolution = 1.875 × 1.875 mm, slice thickness = 8 mm, spin-lock frequency = 10 Hz (corresponding to an amplitude of ~235 nT), and spin-lock duration = 125 ms (corresponding to a 1¼ turn of the magnetization around the y'-axis, as illustrated in Figure 1D). Because our technique is sensitive to the phase of the oscillating current relative to the spin-lock pulse, a TR of 1.0125 s was chosen, so that this phase would systematically vary across the different TRs within each run.

To determine the *specificity* of our technique, the oscillating-current amplitude was set to 2.5 mA while its frequency was varied from 4 to 17 Hz, changing every 15 TRs within a single run. To determine the *sensitivity* of our technique, the oscillating-current frequency was set to 10 Hz while its amplitude was varied from 0 to 0.05 mA, changing every 15 TRs within a single run. The magnitudes of the magnetic field at the center of the slice (1 cm from the center of the wire loop) corresponding to current amplitudes of 0 to 0.05 mA were calculated by using the Biot-Savart law and ranged from 0 to 1.2 nT. The signal intensity was averaged in a 9 × 9 voxel region-of-interest (ROI) at the center of the loop, and a sinusoidal function was fit to the 15 TRs corresponding to each oscillating-current frequency and amplitude. The amplitude of this sinusoid was then plotted as a function of the current frequency (with amplitude held constant) or as a function of the current amplitude (with frequency held constant). A 1-tailed paired t-test was performed between the amplitude of the sinusoid at 0 mA, and the amplitude of the sinusoid at

each of the other current amplitudes to determine the smallest magnetic field detectable. Magnetic fields for which the corresponding *P*-value was smaller than 0.01 were considered detectable.

2.3 | Human experiments

We then performed in vivo experiments to demonstrate the ability of our technique to image functional modulations of neuroelectric oscillations in the alpha-band (8-12 Hz), which comprise a particularly important neuro-oscillatory functional activity pattern in the brain. More specifically, we examined modulations of activity in this frequency band induced by alternately opening and closing the eyes, which is known to strongly modulate alpha activity in visual cortex (larger when eyes are closed)[31,32] and which has been shown to result in a mean peak frequency for alpha power of 9.9 ± 1.0 Hz in a study of 110 adults.[33] All subjects provided written informed consent to participate in the experiments, which were carried out in accordance with protocols approved by the Duke University Health System Institutional Review Board.

2.4 | Human EEG experiment

Before running the MRI experiments, we performed EEG measurements of alpha activity in response to alternations between eye closure and eye opening on a healthy volunteer to confirm the alpha modulation and to delineate the temporal characteristics of that modulation. The participant was given a spoken word cue to close their eyes, followed by another cue 4 s later to open their eyes, and then alternating every 4 s for a total of 82 trials. Data were acquired and analyzed as described in the Supporting Information, which is available online.

2.5 | Human MRI experiments: data acquisition

We then performed MRI experiments in 8 healthy volunteers to demonstrate the ability of our technique to tomographically image functional modulations of neuroelectric oscillations in the alpha-band. As in the EEG experiment, the subjects were instructed to alternately open and close their eyes every 4 s to modulate the alpha activity in their visual cortex.

Spin-lock techniques are sensitive to spatiotemporal variations of the static magnetic field B_0, including those induced in the brain by breathing, potentially resulting in confounding signal modulations at the breathing frequency.[34] Accordingly, to rule out any contribution from such a source, the subjects were trained to alternatively breathe in and out within 2 s and hold their breath for 2 s to ensure that such breathing-induced signal modulations would occur at a higher frequency (0.25 Hz and higher harmonics) than the 0.125-Hz eyes-open/eyes-closed task frequency that would modulate the alpha power.

For each subject, 4 runs were acquired with this paradigm, using a 10-Hz spin-lock frequency centered on the alpha-band (Figure 2A). To contrast with these NEMO runs, 2 control runs were acquired with the same eyes-open/eyes-closed paradigm, but using a 30-Hz spin-lock frequency (control-1; Figure 2B). Two additional control runs were also acquired using the same 10-Hz spin-lock frequency as for the NEMO runs, but while the subjects kept their eyes open continuously (control-2; Figure 2C), except for some occasional blinking, which would not have modulated alpha activity at 0.125 Hz. Finally, 1 run optimized for recording BOLD activity was acquired with the eyes-open/eyes-closed paradigm, but using no spin-lock preparation and with a longer TE (Figure 2D).

These experiments were performed on the 3T MRI scanner with a 32-channel head coil (Nova Medical, Wilmington, MA). T_1-weighted anatomical images of the whole brain were acquired with a 3D inversion-prepared spoiled gradient-echo sequence. The fMRI data were then acquired in a single axial slice along the calcarine fissure, with TR = 500 ms, TE = 3 ms (for the NEMO and control runs, to minimize any BOLD effect) or 30 ms (for the BOLD runs), FOV = 24 × 24 cm, matrix size = 64 × 64, in-plane spatial resolution = 3.75 × 3.75 mm, slice thickness = 8 mm (to adequately cover the primary visual cortex), and scan time = 4 min 16 s. For the NEMO and control runs, the spin-lock duration was set to 125 ms, as in the phantom experiments.

The subjects were shown a fixation cross at the center of a black screen through a projector. They used both visual cues (a color change of the cross every 2 s) and auditory cues

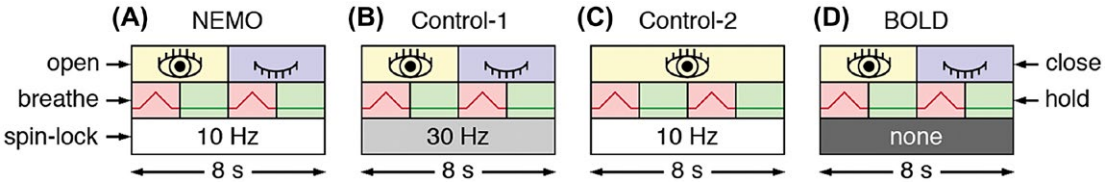

FIGURE 2 Paradigms. A, NEMO runs using a 10-Hz spin-lock frequency to detect neuroelectric oscillations in the alpha-band (8-12 Hz), a 0.125-Hz eyes-open/eyes-closed paradigm to modulate the alpha-band activity, and a 0.25-Hz controlled breathing to minimize physiological noise. B, Control-1 runs using a 30-Hz spin-lock frequency. C, Control-2 runs using eyes open continuously. D, BOLD runs using no spin-lock preparation and a longer TE

(from the scanner sounds) to determine when to open or close their eyes and when to breathe or hold their breath. All subjects practiced the task before the MRI scans. The NEMO, control-1, control-2, and BOLD runs were interleaved.

2.6 | Human MRI experiments: data analysis

In contrast to the phantom experiments, in which the oscillating-current frequency or amplitude was systematically varied across a wide range of values to determine the specificity and sensitivity of our technique, the goal of the human experiments was to demonstrate our ability to image functional modulations of neuroelectric oscillations between 2 conditions (eyes-open versus eyes-closed), analogous to how functional modulations are typically investigated in BOLD fMRI studies. Thus, the data were analyzed by taking a Fourier transform (FT) along the time course of each voxel in each run and by looking for a peak at the 0.125-Hz eyes-open/eyes-closed task frequency, which was expected to be observed in the NEMO runs but not in the control runs. Our paradigm and analysis were focused on the functional modulation induced at 0.125 Hz by our task manipulation (more versus less alpha activity during the eyes-closed versus eyes-open periods, respectively), not on the activity at the 10-Hz spin-lock frequency itself, which did not correspond to our functional task. This FT analysis was more effective at picking up the 0.125-Hz task frequency in the power spectrum than a traditional general linear model analysis, which would have required assumptions to be made on the exact shape of the NEMO response function.

Activation maps were generated by extracting the magnitude of the FT at 0.125 Hz. Although the NEMO runs were optimized to detect the NEMO signal, they could still have had some sensitivity to residual hemodynamic confounds (e.g., BOLD or inflow effects) or physiological confounds (e.g., breathing-induced signal fluctuations). To minimize such confounds, 3 additional postprocessing steps, consisting of a regression, filtering, and rectification (RFR), were performed before taking the FT, as described below. This procedure took advantage of the different temporal characteristics of these signals. Specifically, any residual hemodynamic and physiological confounds would be expected to show a cyclic signal fluctuation at the 0.125-Hz eyes-open/eyes-closed task frequency (Figure 3A) or at the 0.25-Hz controlled breathing frequency, because such effects would tend to cause only slow (relative to the neuronal oscillations in the alpha-band and to the spin-lock frequency) changes in the local deoxyhemoglobin concentration, magnetic susceptibility, magnetic field, and longitudinal magnetization of the NEMO signal.

In contrast, the NEMO signal, which is sensitive to the phase of the neuroelectric oscillations relative to the spin-lock pulse, as shown in our phantom experiments, may have 2 components. If the neuroelectric oscillations and spin-lock pulse are exactly in-phase at each TR across a run (e.g., both at 10 Hz), the NEMO signal is expected to show a cyclic pattern at the eyes-open/eyes-closed task frequency (constant-phase NEMO signal). On the other hand, if there are large phase variations at the different TRs, the NEMO signal is expected to have a low versus high standard deviation, but constant mean, during the eyes-open versus eyes-closed periods, respectively (random-phase NEMO signal; Figure 3B). In this study, the NEMO signal due to neuroelectric oscillations in the alpha-band was expected to contain a substantial random-phase component, because such oscillations spanned a frequency range of 8-12 Hz and because there were inherent temporal variations between the onset of each visual-task event (opening or closing of the eyes in response to the cue) and the spin-lock pulses.

The RFR procedure consisted of the following 3 steps. First, a cortical parcellation of the T_1-weighted anatomical images was performed with FreeSurfer[35] based on the Destrieux atlas,[36] resulting in 74 cortical parcels per hemisphere. These parcels were resampled from the FreeSurfer

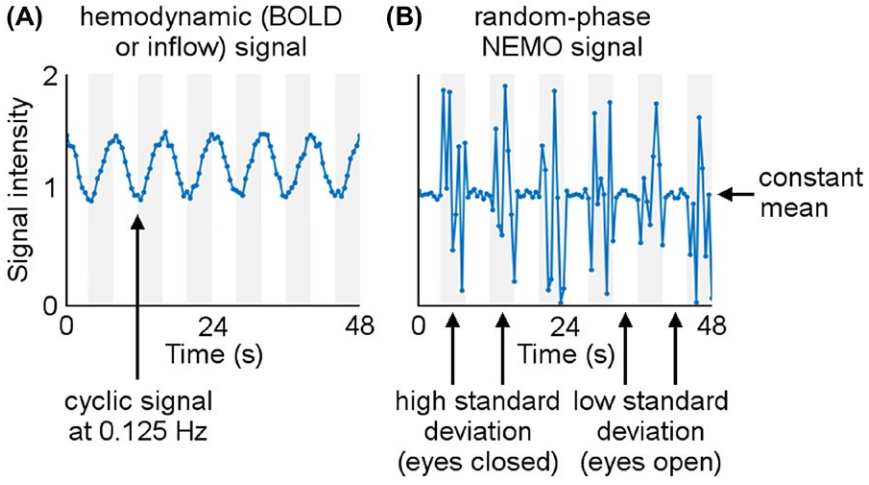

FIGURE 3 A, Simulated time course for a hemodynamic signal (e.g., BOLD or inflow effects), showing a cyclic signal fluctuation at the 0.125-Hz eyes-open/eyes-closed task frequency. B, Simulated time course for a random-phase NEMO signal, showing a low versus high standard deviation, but constant mean, during the eyes-open periods (white stripes) versus eyes-closed periods (gray stripes), respectively

mesh to the MRI slice and merged across both hemispheres to yield different ROIs. For each run and each ROI, the time course was averaged across the voxels within each ROI and then regressed out from the time course of each voxel within the ROI. This step reduced any slow cyclic hemodynamic and physiological confounds, while preserving any random-phase NEMO signal that varied across different voxels within an ROI. Such a regression based on the MRI signal in different ROIs was found to be more effective at removing breathing-induced signal fluctuations in the brain voxels than a regression based on a single respiratory signal recorded from a respiratory belt, as the breathing-induced signal fluctuations in the brain are not directly proportional to the single respiratory signal from the belt.

Second, a high-pass filter with a cutoff frequency of 0.3 Hz (just above the 0.25-Hz controlled breathing frequency and higher than the 0.125-Hz eyes-open/eyes-closed task frequency) was applied to further reduce any residual low-frequency signal that was not regressed out in the previous step. Importantly, the regression and filtering steps of the RFR procedure did not eliminate the random-phase NEMO signal, because such a signal had a constant mean and hence no 0.125-Hz frequency component in the power spectrum.

Third, the time course of each voxel was rectified by subtracting the mean over the whole run and taking the absolute value at each TR, which converted the random-phase NEMO signal (with low versus high standard deviation, but constant mean) into a cyclic signal at the 0.125-Hz task frequency, resulting in a peak at that frequency in the power spectrum. Altogether, the RFR procedure enhanced any random-phase NEMO signal, while minimizing any slow cyclic residual hemodynamic and physiological confounds, thereby allowing a clear distinction between the NEMO and BOLD activations.

The RFR procedure was first tested on simulated NEMO and BOLD runs with the same paradigm as used in the human experiments. The simulated BOLD run consisted of

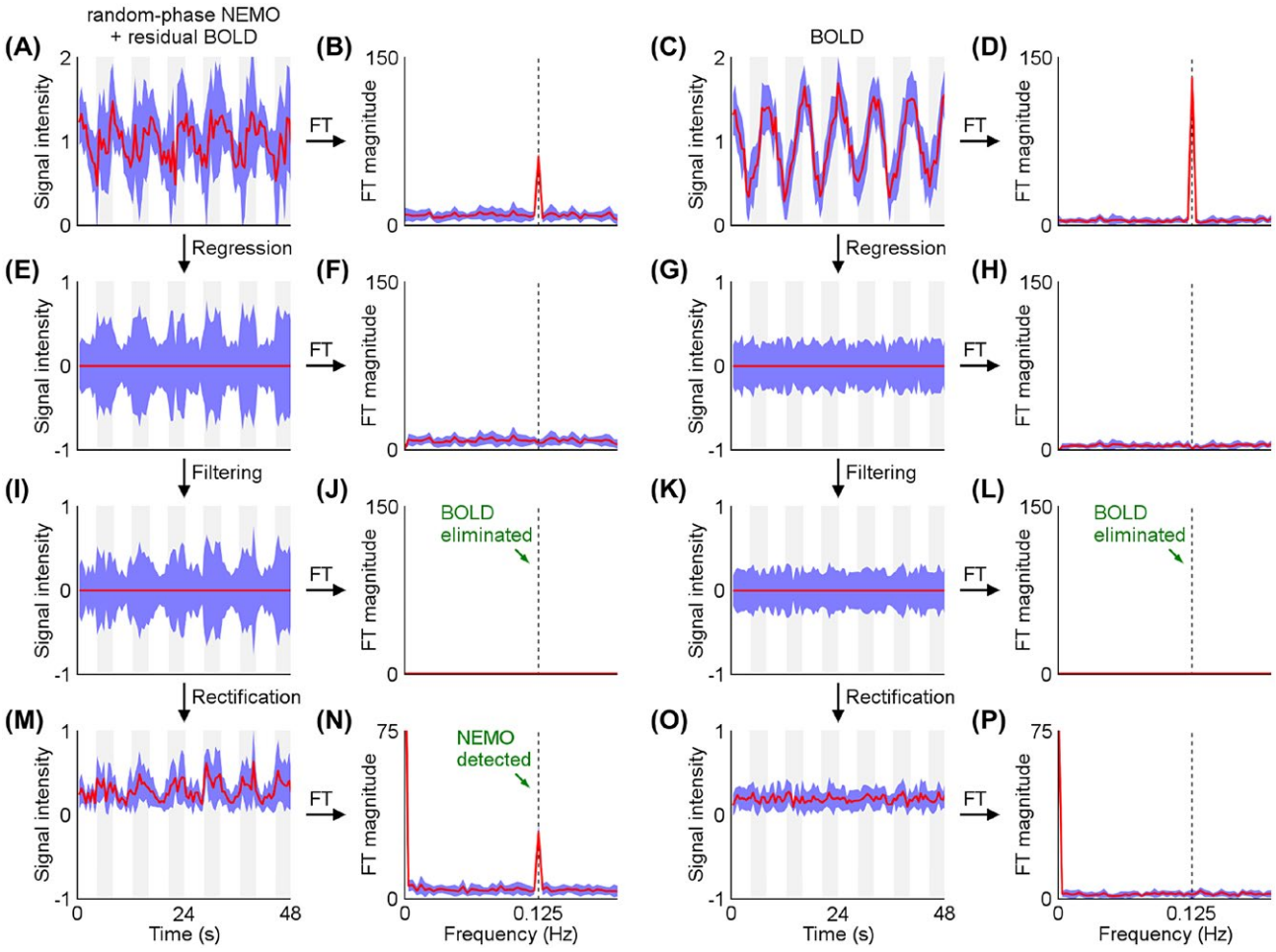

FIGURE 4 A-P, Simulated time courses and power spectra for a NEMO run with random-phase NEMO and residual BOLD signals (left) and for a BOLD run (right), before and after each step of the RFR postprocessing procedure (regression, high-pass filtering, rectification). The red lines represent the mean (arbitrary units), whereas the purple areas represent the mean ± standard deviation. The regression and filtering steps eliminate the slow cyclic BOLD signal at the 0.125-Hz task frequency (J,L), but not the random-phase NEMO signal, which has a low versus high standard deviation, but constant mean, during the eyes-open (white stripes) versus eyes-closed (gray stripes) periods, respectively (I). The additional rectification step converts the NEMO signal into a cyclic signal at 0.125 Hz (M), resulting in a peak at that frequency in the power spectrum (N)

a canonical BOLD hemodynamic response function (with an amplitude of 1) convolved with a 0.125-Hz square wave, along with additive noise (with a uniform distribution between ±0.5). The simulated NEMO run consisted of the sum of: (i) a time course with a low versus high standard deviation (with a uniform distribution between ±0.5 versus ±1), but constant mean, during the eyes-open versus eyes-closed periods, respectively (random-phase NEMO signal), and (ii) a time course identical to that of the BOLD run (reflecting possible residual BOLD signal). In the simulated NEMO time course, the oscillating magnetic field was not assumed to be at a specific frequency, but could have a range of frequencies (e.g., 8-12 Hz for a spin-lock frequency of 10 Hz), which would all result in a low versus high standard deviation, but constant mean, during the eyes-open versus eyes-closed periods, respectively. A 10-voxel ROI was used for each run. These simulations confirmed that, after RFR, the 0.125-Hz peak is detected in the NEMO run, but is eliminated in the BOLD run (Figure 4). The same procedure was then applied to the experimental human brain data, and new activation maps were generated as described above.

To focus on the activation in the primary visual cortex (V1) and to combine the results across all runs, power spectra were generated by averaging the magnitude of the FT in the same left and right anatomically defined occipital-pole ROIs for the average of all NEMO, control-1, control-2, or BOLD runs from each individual subject, both before and after RFR. These power spectra were then further averaged across all 8 subjects. Additional details are described in the Supporting Information.

3 | RESULTS

3.1 | Phantom MRI experiments

The phantom experiments (Figure 5) demonstrate that our technique can detect magnetic field oscillations in a specifiable frequency band with an FWHM of ~10 Hz (Figure 5A) and with a magnitude as low as 0.06 nT (Figure 5B). They also confirm that the NEMO signal depends on the phase of the magnetic field oscillations relative to the spin-lock pulse (Figure 5C).

3.2 | Human EEG experiment

The EEG experiment (Figure 6) delineated the time course of the task-induced modulations in alpha power over visual cortex, showing the power to rapidly increase or decrease ~700 ms after the cue to close versus open the eyes, respectively (Figure 6A). Given this time frame, we chose a TR of

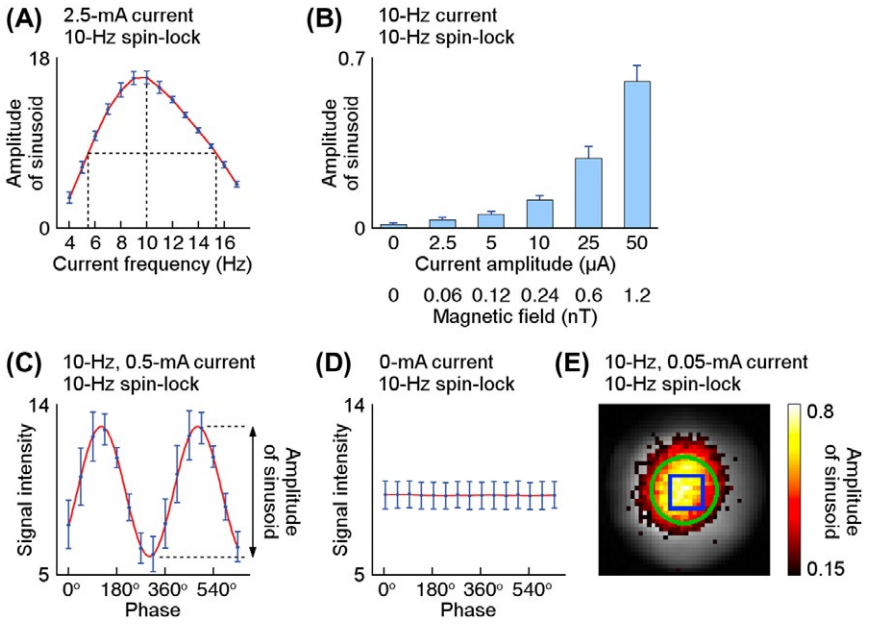

FIGURE 5 Phantom experiments demonstrating the specificity, sensitivity, and phase dependence of our spin-lock technique. Amplitude of the fitted sinusoid (mean ± standard deviation, arbitrary units) versus the current frequency (A), showing a peak centered on the spin-lock frequency (here, 10 Hz) with a ~10 Hz FWHM, or versus the current amplitude (B), showing that a magnetic field as low as 0.06 nT can be detected ($P = 0.0002$, uncorrected), which corresponds to 2.6 pT when using the same voxel size and number of TRs as in our human experiments. C, Signal intensity (mean ± SD, arbitrary units) versus the phase of the oscillating current relative to the spin-lock pulse, fit with a sinusoid. D, Signal intensity with no oscillating current applied, fit with a sinusoid. E, Amplitude of the fitted sinusoid in each voxel (arbitrary units) overlaid on an image of the phantom. The green circle shows the wire loop (1 cm from this axial slice and generating an oscillating magnetic field primarily orthogonal to the slice), whereas the blue square shows the ROI

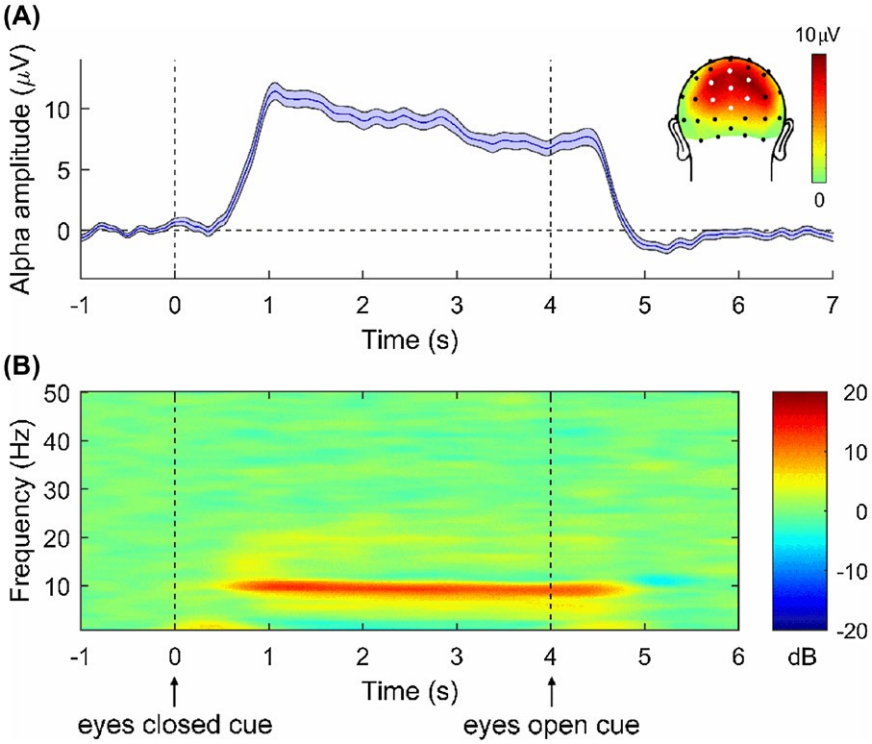

FIGURE 6 EEG measurements of alpha activity change for eyes-closed versus eyes-open. A, Time course (mean ± standard error of the mean) of the magnitude change of the alpha-band oscillatory activity (8-12 Hz) from a group of electrode sites (white dots on the accompanying topographic head plot) over parietal-occipital scalp, centered around scalp site POz (center white dot on the head plot), time-lock-averaged over all trials, showing a rapid increase starting at ~700 ms after the cue to close the eyes (time 0). The topographic head plot insert in the panel shows the increase in the alpha-band magnitude from these parietal-occipital scalp sites, averaged over a 1000-4500 ms time window after the cue to close the eyes, relative to the eyes-open periods. B, Time-frequency plot of the time-locked power change from these same electrodes, showing that the alpha-band change modulated by the eyes-open/eyes-closed task is by far the largest effect seen, and is distinctly selective to a band around 10 Hz

500 ms for the MRI experiments to capture this change in the magnitude of the alpha-band oscillations. Furthermore, a time-frequency plot of the time-locked power change over posterior scalp shows that the alpha change modulated by the eyes-open/eyes-closed task is by far the largest effect seen, and is distinctly selective around 10 Hz (Figure 6B).

3.3 | Human MRI experiments

Activation maps in 2 representative subjects from the human MRI experiments (Figure 7) are shown unthresholded to illustrate the full range of activity at the task frequency. Before the RFR postprocessing procedure, the NEMO runs, which were acquired with the eyes-open/eyes-closed paradigm using a 10-Hz spin-lock frequency centered on the alpha-band, demonstrated substantial activations in the visual cortex (Figure 7A, green ovals). The control-1 runs, which were acquired with the same eyes-open/eyes-closed paradigm, but using a 30-Hz spin-lock frequency, generally showed little activation in the visual cortex (Figure 7B), consistent with there being no overlap between the alpha-band activity being modulated by the eyes-open/eyes-closed task and the frequency range to which a 30-Hz spin-lock is sensitive. The control-2 runs, which were acquired using the same 10-Hz spin-lock frequency as for the NEMO runs, but while the subjects kept their eyes open continuously, also generally showed little activation in the visual cortex (Figure 7C), consistent with there being no modulation of alpha activity in this condition. As expected, the BOLD runs, which were acquired with the same eyes-open/eyes-closed paradigm as for the NEMO runs, but using no spin-lock preparation and with a longer TE, showed substantial BOLD activations in the visual cortex (Figure 7D, green ovals).

After performing the RFR postprocessing procedure to minimize any slow cyclic residual hemodynamic and physiological confounds and to enhance any random-phase NEMO signal, the control-1 (Figure 7F), control-2 (Figure 7G), and BOLD (Figure 7H) runs generally showed no activations in the visual cortex, whereas substantial activations remained in the NEMO runs, particularly in the occipital-pole/V1 region in both hemispheres (Figure 7E, green ovals). The activation maps in the rest of the slice could show some differences before versus after RFR and/or across subjects, because the activation before versus after RFR did not reflect the same signal, because the activation maps were normalized separately to highlight any activation in the visual cortex (see

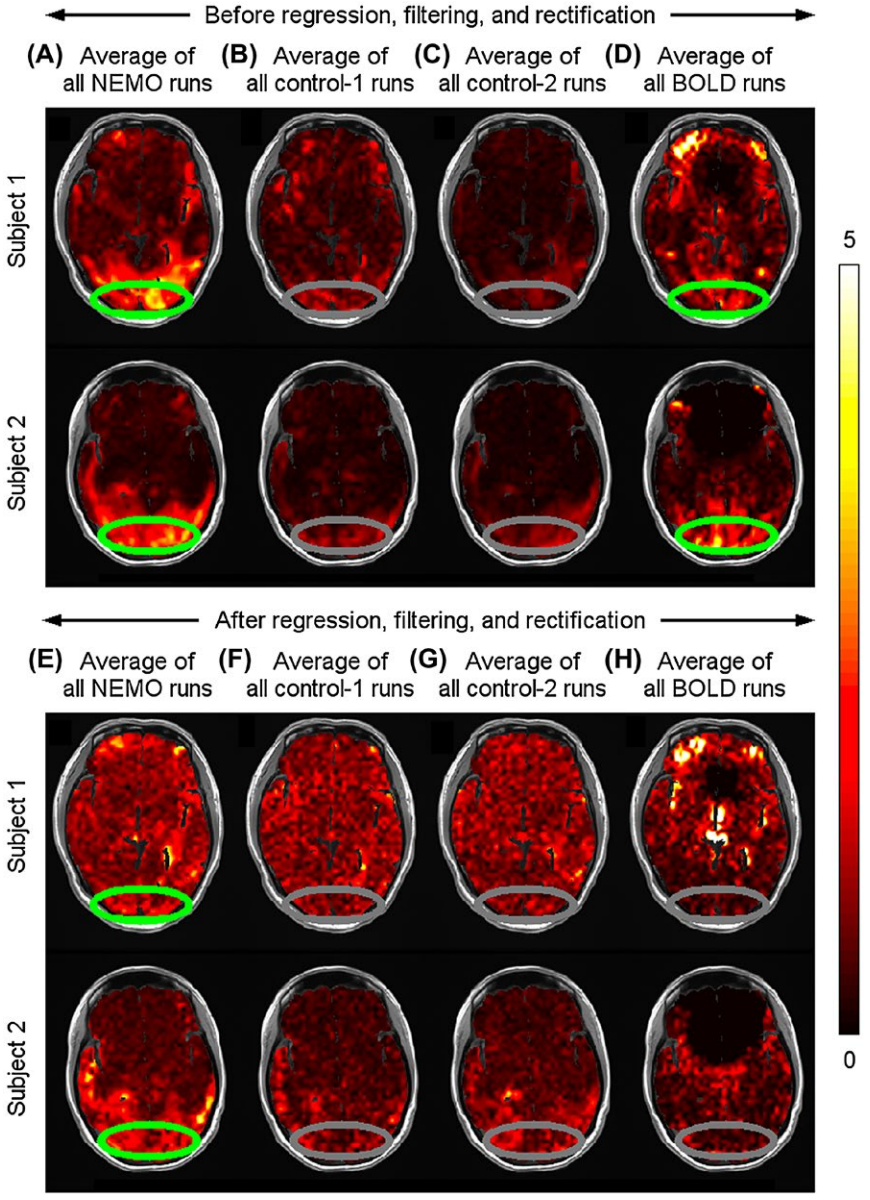

FIGURE 7 Activation maps from all conditions in 2 representative subjects. A-D, Maps of the FT magnitude at 0.125 Hz (arbitrary units) before the RFR postprocessing procedure, showing substantial activations in the visual cortex for the NEMO (A, green ovals) and BOLD (D, green ovals) runs relative to the control-1 (B) or control-2 (C) runs. E-H, Corresponding activation maps after RFR, showing no or little activation for the control-1 (F), control-2 (G), and BOLD (H) runs, but still substantial activations for the NEMO runs (E, green ovals), particularly in the occipital-pole/V1 region in the acquired slice and whose spatial distributions differed from the BOLD activation before RFR (D)

Supporting Information), and because the subjects could have had different head tilts.

In addition, the NEMO activation (after RFR) and the BOLD activation (before RFR) could have somewhat different activation patterns for two reasons. First, the NEMO and BOLD *runs* were optimized to detect the NEMO and BOLD signals, respectively (and the NEMO runs were further processed with the RFR procedure to minimize any contribution from residual hemodynamic effects). Second, the NEMO and BOLD *signals* arise from different neuronal mechanisms. Specifically, the BOLD activation (before RFR), which reflects hemodynamic modulations resulting from the *visual input* induced by the eyes-open/eyes-closed task, would tend to be observed in the visual cortex, mostly in the gray matter, including in V1 and higher visual cortical areas (Figure 7D). In contrast, the NEMO activation (after RFR), which would be expected to reflect modulations of *neuronal oscillations in the alpha-band* that are well known to also be induced by the eyes-open/eyes-closed task, could extend throughout the occipital gray matter beyond these regions (Figure 7E). Nevertheless, we used a common ROI (the anatomically defined occipital-pole/V1 ROI) to compare the activation from these two contrast mechanisms.

Before RFR, and as expected, the power spectra averaged in this ROI (Figure 8A) generally showed a clear 0.125-Hz peak for the NEMO (Figure 8B), control-1 (Figure 8C), and BOLD (Figure 8E) runs, but not for any of the control-2 runs (Figure 8D). Although the NEMO and control-1 runs were acquired with a TE of 3 ms to minimize any BOLD effect, they could still have had some sensitivity to hemodynamic effects (e.g., residual BOLD or inflow effects) or some physiological confounds at the 0.125-Hz eyes-open/eyes-closed task frequency, which thus could have contributed to such a peak. In contrast, the control-2 runs, in which

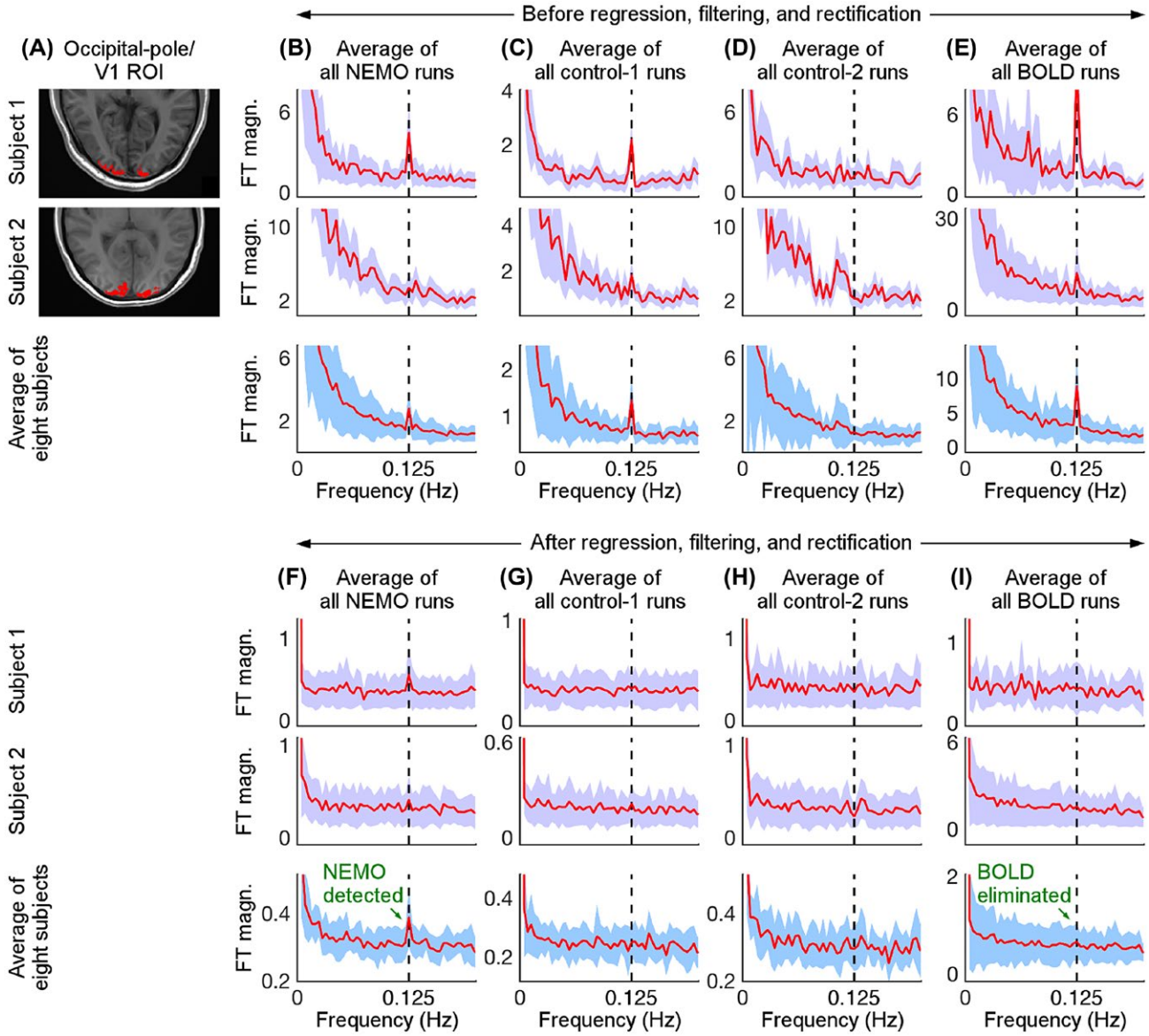

FIGURE 8 Power spectra from all conditions in the occipital-pole/V1 ROIs for the 2 representative subjects shown in Figure 7 and for the average across all 8 subjects. A, Anatomically defined occipital-pole/V1 ROIs. B-I, FT magnitude in these ROIs for the average of all NEMO, control-1, control-2, and BOLD runs, both before (B-E) and after (F-I) the RFR procedure. The red lines represent the mean FT magnitude (arbitrary units), the purple areas represent the mean ± standard deviation across all the voxels in that subject's ROI, and the blue areas represent the mean ± standard deviation across the 8 subjects of the mean FT magnitude in each subject's ROI. These results show a local peak at the 0.125-Hz eyes-open/eyes-closed task frequency in the NEMO runs after RFR for the 2 individual subjects, which was enhanced when averaged across all 8 subjects (F, last row), further supporting its neuroelectric origin. In contrast, the 0.125-Hz peak was eliminated by the RFR procedure in the BOLD runs, both for the 2 individual subjects and for the average across all subjects (I), confirming its hemodynamic origin. After RFR, the 0.125-Hz peak was also absent in the control-1 (G) and control-2 (H) runs

the eyes were always open, would not have been affected by such confounds.

After RFR, the 0.125-Hz peak was manifest in the NEMO runs (Figure 8F), but was absent in the control-1 (Figure 8G), control-2 (Figure 8H), and BOLD (Figure 8I) runs, as predicted and as confirmed by our simulations (Figure 4). The NEMO peak after RFR was not clearly detected in every single subject, possibly because of the variability in the magnitude of the alpha-band oscillations across subjects. However, the power spectra averaged across all 8 subjects (Figure 8F-I, last row) showed a very clear 0.125-Hz peak for the NEMO runs, but no such peak for the control-1, control-2, or BOLD runs. In the power spectra averaged across all NEMO runs and all 8 subjects, the height of the 0.125-Hz peak relative to the baseline was 1.21 before RFR (Figure 8B) and 0.077 after RFR (Figure 8F).

The activation maps (Figure 7) represent the power at 0.125 Hz in all voxels, whereas the power spectra (Figure

8) represent the power in the occipital-pole/V1 ROI at all frequencies, so they will not necessarily be closely aligned. Importantly, voxels with a higher magnitude in the activation maps do not necessarily have a peak at 0.125 Hz in the power spectra, so the presence or absence of such a peak (relative to other frequencies) is a particularly relevant characteristic to bear in mind.

Statistical analyses (see Supporting Information) performed across all 8 subjects showed that, after RFR, there was a significant 0.125-Hz peak for the NEMO runs ($P = 0.0086$), but not for the control-1 ($P = 0.2019$), control-2 ($P = 0.8459$), or BOLD ($P = 0.1153$) runs, in the occipital-pole/V1 ROI. Similar analyses performed across 7, 6, or 5 subjects for all possible combinations of subjects (Supporting Information Figure S1) showed that there was still a significant ($P < 0.05$) 0.125-Hz peak for the NEMO runs in 100%, 100%, and 57% of the combinations, respectively, but no such peak for the control-1, control-2, or BOLD runs in nearly all combinations.

Additional analyses performed across all 8 subjects showed that, after RFR, the power at 0.125 Hz was significantly higher for the NEMO runs relative to the control-1 ($P = 0.0001$) and control-2 ($P = 0.0026$) runs in the occipital-pole/V1 ROI. Similar analyses performed across 7, 6, or 5 subjects (Supporting Information Figure S2) showed that the power at 0.125 Hz remained significantly higher ($P < 0.05$) for the NEMO runs relative to the control-1 and control-2 runs in all combinations.

Finally, other anatomically defined ROIs located in more anterior brain regions (Supporting Information Figure S3) showed no significant 0.125-Hz peaks for any of the NEMO, control-1, control-2, or BOLD runs after RFR.

4 | DISCUSSION AND CONCLUSIONS

These results suggest that our new MRI technique has the sensitivity and specificity to noninvasively image local magnetic field oscillations in vivo resulting from neuroelectric activity in specifiable frequency bands (here, the alpha-band). The control experiments showed that there was no such activation when the spin-lock frequency was outside the alpha-band (control-1) or when there was no modulation of alpha activity because the eyes were kept open (control-2). The control-2 runs, which used the same 10-Hz spin-lock frequency as the NEMO runs, further ruled out any contribution from B_0/B_1 inhomogeneities, given that such inhomogeneities would not have been synchronized with the eyes-open/eyes-closed task. Finally, the experimental paradigm and postprocessing steps were specifically designed to minimize any slow cyclic residual hemodynamic and physiological confounds (e.g., breathing-induced signal fluctuations). A comparison with conventional BOLD fMRI suggests that the NEMO activation in this study likely reflects task-based modulations of neuroelectric oscillatory activity in the alpha-band, rather than any residual hemodynamic effects, physiological noise, or B_0/B_1 inhomogeneities. Importantly, while both the NEMO and BOLD signals were modulated and detected at the 0.125-Hz eyes-open/eyes-closed task frequency (Figure 8F versus 8E), the phantom experiments (Figure 5A and C) and the NEMO versus control-1 runs in the human experiments (Figure 8F versus 8G) demonstrate that our technique can detect magnetic field oscillations in a specifiable frequency band and sample the temporally varying phase of the oscillation itself, which BOLD fMRI cannot directly sample, because it is inherently limited by the sluggishness of the hemodynamic response.

Previous phantom experiments based on other spin-lock techniques[24,26] reported sensitivities of 1 and 0.25 nT, which corresponds to 17.6 and 0.56 nT when using the same voxel size and number of TRs we used in our phantom experiments. In contrast, the sensitivity measured in our phantom experiments was 0.06 nT (Figure 5B), representing a substantial improvement. When taking into account the larger voxel size (3.75 versus 1.875 mm in-plane resolution) and number of TRs (512 versus 15) used in our human experiments, resulting in a factor of sqrt(512/15) × 4 larger SNR, this 0.06-nT value actually corresponds to 2.6 pT, which is comparable to somatic-evoked magnetic fields measured with MEG above the primary somatosensory cortex of the piglet.[37] After further considering the 3.4-fold lower temporal SNR due to the presence of physiological noise in the human, but not phantom, experiments (43.7 versus 147.9), it is expected that our technique can still image both spontaneous and event-induced functional neuroelectric oscillations, which have been estimated to generate local magnetic fields of 0.1 nT or larger in a typical voxel.[38,39]

In this initial study, we chose to first image neuroelectric oscillations in the alpha-band, because of its functional importance and widespread occurrence in the human brain and because its power variations are of particularly strong amplitude in humans and could be induced with a straightforward eyes-open/eyes-closed task.[31,32] However, our technique can in principle be extended to image neuroelectric oscillations, both event-induced and spontaneously generated, in other frequency bands (e.g., theta, beta, gamma) by setting the spin-lock frequency accordingly. Furthermore, our phantom experiments (Figure 5B) demonstrate that this technique has the potential sensitivity to image neuroelectric oscillations considerably smaller than the ones shown here, such as those induced by sensory or cognitive events. Another whole class of neuroelectric oscillations that could be very effectively imaged with this technique would be those driven by steady-state stimulus presentation, such as steady-state visual evoked potentials,[40] where the spin-lock frequency could be tuned to the specific frequency of the stimulus presentation.

Lastly, although not all neuronal activities are oscillatory, neuronal oscillations represent an extensive and far-reaching class of neural activity patterns that are thought to play key roles in perceptual, cognitive, and interregional-control processes (e.g., attentional control).[41-44] Accordingly, the ability to noninvasively image such oscillatory neuronal activities with high spatial and temporal specificity will be highly impactful for the study of the neural mechanisms underlying both normal and abnormal cognitive functions.

A current limitation of our technique is that it cannot detect nonoscillatory neuroelectric activity or distinguish between neuroelectric oscillations with close frequencies (within the ~10 Hz FWHM of the response curve; Figure 5A). However, with further development, it could potentially detect modulations of neuroelectric oscillations across a frequency band that is wider than ~10 Hz by using a ramped spin-lock pulse spanning the desired frequency range.[25] In addition, our initial study used a controlled-breathing paradigm, with a breathing frequency substantially higher than the eyes-open/eyes-closed task frequency, to clearly separate the two corresponding peaks in the power spectra and thereby unambiguously demonstrate that the NEMO activation was not due to breathing-induced B_0 fluctuations. In future studies, however, the RFR procedure alone can be used or our technique can be further developed to incorporate a B_0-insensitive spin-lock preparation,[34] dynamic shimming, and/or low-field imaging to reduce or eliminate sensitivity to B_0 fluctuations, thereby allowing the use of free-breathing paradigms and thus much wider applicability. Finally, while the RFR procedure was designed to minimize any slow cyclic residual hemodynamic and physiological confounds at the 0.125-Hz eyes-open/eyes-closed task frequency, there could potentially also have been some residual hemodynamic or physiological confounds that were not manifested as slow cyclic signals and that were not minimized by the RFR procedure.

This initial proof-of-concept study only represents the first step toward validating our new technique, and several additional experiments will be needed to fully validate it, to investigate its spatial and temporal specificity, to further improve its sensitivity, to address its current limitations, and to assess its performance in a wider range of applications (e.g., to detect modulations of neuroelectric oscillations in different frequency bands, between which the spin-lock duration and sensitivity may differ). For example, one additional validation experiment should use a longer eyes-open/eyes-closed cycle (e.g., 20 s rather than the 8 s used here) to demonstrate the rapid onset of the NEMO signal with no interference from residual hemodynamic effects induced in the previous cycle and to unambiguously assess the relative timing of the NEMO versus BOLD signal changes.

Nevertheless, our initial results provide evidence suggesting that MRI can be used to noninvasively and directly image neuroelectric oscillations in the human brain in vivo. This new technique should not be viewed as being aimed at replacing existing neuroimaging techniques, which can address a wide range of questions, but it is expected to be able to image functionally important neural activity in ways that no other technique can currently achieve. Specifically, it is designed to *directly* image neuroelectric activity, and in particular *oscillatory* neuroelectric activity, which BOLD fMRI cannot directly sample, because it is intrinsically limited by the temporal smear and temporal delay of the hemodynamic response. Furthermore, it has the potential to do so with a high and unambiguous spatial specificity, which EEG/MEG cannot achieve, because of the limitations of the inverse problem. We expect that our technique can be extended and optimized to directly image a broad range of intrinsic and driven neuronal oscillations, thereby advancing our ability to study neuronal processes, both functional and dysfunctional, in the human brain.

ACKNOWLEDGMENTS

We thank A.V. Avram for his assistance with programming a preliminary version of the pulse sequence, C. Petty for his assistance with the MELODIC data processing, as well as P.A. Bandettini, G.H. Glover, and L.L. Wald for helpful discussions.

REFERENCES

1. Bandettini PA, Wong EC, Hinks RS, Tikofski RS, Hyde JS. Time course EPI of human brain function during task activation. *Magn Reson Med*. 1992;25:390–397.
2. Kwong KK, Belliveau JW, Chesler DA, et al. Dynamic magnetic resonance imaging of human brain activity during primary sensory stimulation. *Proc Natl Acad Sci U S A*. 1992;89:5675–5679.
3. Ogawa S, Tank DW, Menon R, et al. Intrinsic signal changes accompanying sensory stimulation: functional brain mapping with magnetic resonance imaging. *Proc Natl Acad Sci U S A*. 1992;89:5951–5955.
4. Hillyard SA, Hink RF, Schwent VL, Picton TW. Electrical signs of selective attention in the human brain. *Science*. 1973;182:177–180.
5. Hämäläinen M, Hari R, Ilmoniemi RJ, Knuutila J, Lounasmaa OV. Magnetoencephalography – theory, instrumentation, and applications to noninvasive studies of the working human brain. *Rev Mod Phys*. 1993;65:413–497.
6. Bodurka J, Jesmanowicz A, Hyde JS, et al. Current-induced magnetic resonance phase imaging. *J Magn Reson*. 1999;137:265–271.
7. Bodurka J, Bandettini PA. Toward direct mapping of neuronal activity: MRI detection of ultraweak, transient magnetic fields changes. *Magn Reson Med*. 2002;47:1052–1058.
8. Park TS, Lee SY, Park J-H, Cho MH, Lee SY. Observation of the fast response of a magnetic resonance signal to neuronal activity: a snail ganglia study. *Physiol Meas*. 2006;27:181–190.
9. Petridou N, Plenz D, Silva AC, et al. Direct magnetic resonance detection of neuronal electrical activity. *Proc Natl Acad Sci U S A*. 2006;103:16015–16020.

10. Sundaram P, Nummenmaa A, Wells W, et al. Direct neural current imaging in an intact cerebellum with magnetic resonance imaging. *NeuroImage*. 2016;132:477–490.
11. Bandettini PA, Petridou N, Bodurka J. Direct detection of neuronal activity with MRI: fantasy, possibility, or reality? *Appl Magn Reson*. 2005;29:65–88.
12. Bianciardi M, Di Russo F, Aprile T, Maraviglia B, Hagberg GE. Combination of BOLD-fMRI and VEP recordings for spin-echo MRI detection of primary magnetic effects caused by neuronal currents. *Magn Reson Imaging*. 2004;22:1429–1440.
13. Chow LS, Cook GG, Whitby E, Paley MNJ. Investigation of axonal magnetic fields in the human corpus callosum using visual stimulation based on MR signal modulation. *J Magn Reson Imaging*. 2007;26:265–273.
14. Chu R, de Zwart JA, van Gelderen P, et al. Hunting for neuronal currents: absence of rapid MRI signal changes during visual-evoked response. *NeuroImage*. 2004;23:1059–1067.
15. Konn D, Gowland P, Bowtell R. MRI detection of weak magnetic fields due to an extended current dipole in a conducting sphere: a model for direct detection of neuronal currents in the brain. *Magn Reson Med*. 2003;50:40–49.
16. Konn D, Leach S, Gowland P, Bowtell R. Initial attempts at directly detecting alpha wave activity in the brain using MRI. *Magn Reson Imaging*. 2004;22:1413–1427.
17. Luo Q, Jiang X, Gao J-H. Detection of neuronal current MRI in human without BOLD contamination. *Magn Reson Med*. 2001;66:492–497.
18. Mandelkow H, Halder P, Brandeis D, et al. Heart beats brain: the problem of detecting alpha waves by neuronal current imaging in joint EEG–MRI experiments. *NeuroImage*. 2007;37:149–163.
19. Parkes LM, de Lange FP, Fries P, Toni I, Norris DG. Inability to directly detect magnetic field changes associated with neuronal activity. *Magn Reson Med*. 2007;57:411–416.
20. Sundaram P, Wells WM, Mulkern RV, et al. Fast human brain magnetic resonance responses associated with epileptiform spikes. *Magn Reson Med*. 2010;64:1728–1738.
21. Tang L, Avison MJ, Gatenby JC, Gore JC. Failure to direct detect magnetic field dephasing corresponding to ERP generation. *Magn Reson Imaging*. 2008;26:484–489.
22. Xiong J, Fox PT, Gao JH. Directly mapping magnetic field effects of neuronal activity by magnetic resonance imaging. *Hum Brain Mapp*. 2003;20:41–49.
23. Redfield AG. Nuclear magnetic resonance saturation and rotary saturation in solids. *Phys Rev*. 1955;98:1787.
24. Witzel T, Lin F-H, Rosen BR, Wald LL. Stimulus-induced rotary saturation (SIRS): a potential method for the detection of neuronal currents with MRI. *NeuroImage*. 2008;42:1357–1365.
25. Halpern-Manners NW, Bajaj VS, Teisseyre TZ, Pines A. Magnetic resonance imaging of oscillating electrical currents. *Proc Natl Acad Sci U S A*. 2010;107:8519–8524.
26. Jiang X, Sheng J, Li H, et al. Detection of subnanotesla oscillatory magnetic fields using MRI. *Magn Reson Med*. 2016;75:519–526.
27. Zhu B, Witzel T, Jiang S, et al. Selective magnetic resonance imaging of magnetic nanoparticles by acoustically induced rotary saturation. *Magn Reson Med*. 2016;75:97–106.
28. Chai Y, Bi G, Wang L, et al. Direct detection of optogenetically evoked oscillatory neuronal electrical activity in rats using SLOE sequence. *NeuroImage*. 2016;125:533–543.
29. Borthakur A, Hulvershorn J, Gualtieri E, et al. A pulse sequence for rapid in vivo spin-locked MRI. *J Magn Reson Imaging*. 2006;23:591–596.
30. Watts R, Andrews T, Hipko S, Gonyea JV, Filippi CG. In vivo whole-brain T1-rho mapping across adulthood: normative values and age dependence. *J Magn Reson Imaging*. 2014;40:376–382.
31. Berger H. Über das Elektrenkephalogramm des Menschen. *Arch Psychiatr Nervenkr*. 1929;87:527–570.
32. Steriade M, Gloor P, Llinás RR, Lopes de Silva FH, Mesulam MM. Basic mechanisms of cerebral rhythmic activities. *Electroencephalogr Clin Neurophysiol*. 1990;76:481–508.
33. Wieneke GH, Deinema CH, Spoelstra P, Storm van Leeuwen W, Versteeg H. Normative spectral data on alpha rhythm in male adults. *Electroencephalogr Clin Neurophysiol*. 1980;49:636–645.
34. Witschey WRT Jr, Borthakur A, Elliott MA, et al. Artifacts in T1ρ-weighted imaging: compensation for B_1 and B_0 field imperfections. *J Magn Reson*. 2007;186:75–85.
35. Dale AM, Fischl B, Sereno MI. Cortical surface-based analysis I: segmentation and surface reconstruction. *NeuroImage*. 1999;9:179–194.
36. Destrieux C, Fischl B, Dale A, Halgren E. Automatic parcellation of human cortical gyri and sulci using standard anatomical nomenclature. *NeuroImage*. 2010;53:1–15.
37. Ikeda H, Leyba L, Bartolo A, Wang Y, Okada YC. Synchronized spikes of thalamocortical axonal terminals and cortical neurons are detectable outside the pig brain with MEG. *J Neurophysiol*. 2002;87:626–630.
38. Romani GL. Fundamentals on neuromagnetism. In: Wiliamson S, ed. *Advances in Biomagnetics*. New York: Plenum Press; 1989:33–46.
39. Wikswo JP. Biomagnetic sources and their models. In: Wiliamson S, ed. *Advances in Biomagnetics*. New York: Plenum Press; 1989:1–19.
40. Herrmann CS. Human EEG responses to 1–100 Hz flicker: resonance phenomena in visual cortex and their potential correlation to cognitive phenomena. *Exp Brain Res*. 2001;137:346–353.
41. Worden MS, Foxe JJ, Wang N, Simpson GV. Anticipatory biasing of visuospatial attention indexed by retinotopically specific alpha-band electroencephalography increases over occipital cortex. *J Neurosci*. 2000;20:1–6.
42. Saalmann YB, Pinsk MA, Wang L, Li X, Kastner S. The pulvinar regulates information transmission between cortical areas based on attention demands. *Science*. 2012;337:753–756.
43. Wang XJ. Neurophysiological and computational principles of cortical rhythms in cognition. *Physiol Rev*. 2010;90:1195–1268.
44. Green JJ, Boehler CN, Roberts KC, et al. Cortical and subcortical coordination of visual spatial attention revealed by simultaneous EEG-fMRI recording. *J Neurosci*. 2017;37:7803–7810.

SUPPORTING INFORMATION

Additional supporting information may be found online in the Supporting Information section at the end of the article.

FIGURE S1 *P*-values from *t*-tests performed across 8, 7, 6, or 5 out of 8 subjects (sorted in ascending order for all possible combinations of subjects) comparing the power at 0.125 Hz versus the power at adjacent frequencies,

averaged over all voxels in the occipital-pole/V1 ROI of each subject. After RFR, there was a statistically significant ($P < 0.05$) peak at the 0.125-Hz eyes-open/eyes-closed task frequency for the NEMO runs in 100%, 100%, 100%, and 57% of the combinations, respectively, but no such peak for the control-1, control-2, or BOLD runs in nearly all combinations

FIGURE S2 *P*-values from *t*-tests performed across 8, 7, 6, or 5 out of 8 subjects (sorted in ascending order for all possible combinations of subjects) comparing the power at 0.125 Hz in the NEMO runs versus the power at 0.125 Hz in the control-1 or control-2 runs, averaged over all voxels in the occipital-pole/V1 ROI of each subject. After RFR, the power at 0.125 Hz was significantly higher ($P < 0.05$) for the NEMO runs relative to the control-1 and control-2 runs in all combinations

FIGURE S3 Power spectra from all conditions in 2 additional ROIs for the 2 representative subjects shown in Figures 7-8 and for the average across all 8 subjects. Anatomically-defined ROIs in the subcallosal gyrus (a) and anterior segment of the circular sulcus of the insula (f). (b-e,g-j) FT magnitude in these ROIs for the average of all NEMO, control-1, control-2, and BOLD runs after the RFR procedure. The red lines represent the mean FT magnitude (arbitrary units), the purple areas represent the mean ± standard deviation across all the voxels in that subject's ROI, and the blue areas represent the mean ± standard deviation across the 8 subjects of the mean FT magnitude in each subject's ROI. For subject 2, the BOLD run had no data in the subcallosal gyrus ROI because of susceptibility-induced signal loss in that region. These results show no local peaks at the 0.125-Hz eyes-open/eyes-closed task frequency in any of the NEMO, control-1, control-2, or BOLD runs, both for the 2 individual subjects and for the average across all 8 subjects ($P > 0.05$)

How to cite this article: Truong T-K, Roberts KC, Woldorff MG, Song AW. Toward direct MRI of neuro-electro-magnetic oscillations in the human brain. *Magn Reson Med.* 2019;00:1–14. https://doi.org/10.1002/mrm.27654